A practical approach to *in vivo* quantification of physiological cross-sectional area for human skeletal muscle

Dongwoon Lee[a], Soo Kim[b], Ken Jackson[a], Eugene Fiume[a], Anne Agur[c]

[a]*Department of Computer Science, University of Toronto, Ontario, Canada*
[b]*School of Physical Therapy, University of Saskatchewan, Saskatchewan, Canada*
[c]*Department of Surgery, University of Toronto, Ontario, Canada*

Abstract

Physiological cross-sectional area (PCSA) is an important property used to predict the maximal force capacity of skeletal muscle. A common approach to estimate PCSA uses an algebraic formula based on muscle volume (MV), fascicle length (FL) and pennation angle (PA) that are measured by magnetic resonance imaging (MRI) and ultrasonographic assessments. Due to the limited capability of assessing architecturally complex muscles with these imaging modalities, the accuracy of measurements and ultimately PCSA estimation is compromised. On the other hand, cadaveric modeling provides a more accurate quantification by effectively dealing with the variable complexity of the muscle but it may not be straightforward to directly apply to *in vivo* studies. Thus, the purpose of our study is to provide a practical approach to PCSA estimation for *in vivo* muscle by integrating both cadaveric and ultrasound data. The muscle architecture *in vivo* is approximated by fitting 3D cadaveric data onto 2D ultrasound data of living subjects. The fitted architectural data is used for PCSA quantification. Validation experiments based on synthetic muscle and cadaveric data, respectively, demonstrate 0.4 – 8.4 % errors between original architecture and its approximation, depending on the anatomical complexity. Furthermore, it is shown that, despite the large inter-subject variability of cadaveric data (standard deviation: $\pm$153.2 mm^2), their transformation toward 2D ultrasound data consistently yields a narrow distribution of PCSA estimation (standard deviation: $\pm$24.6 $\sim$ $\pm$35.7 mm^2), which provides a practical insight into accurate quantification of PCSA for *in vivo* muscle.

Keywords: skeletal muscle; muscle architecture; PCSA; ultrasonography; digitization

1. Introduction

Physiological cross-sectional area (PCSA) is an important determinant of peak muscle force production during movement [6]. Since force predictions are known to be highly sensitive to changes in PCSA [3], reliable functional analysis requires accurate determination of this parameter. An algebraic method [1, 15, 12] is commonly used to calculate PCSA based on architectural parameters including muscle volume (MV), fascicle length (FL) and pennation angle (PA). To investigate the architectural parameters *in vivo*, magnetic resonance imaging (MV) and ultrasound (FL, PA) have been used [16, 5, 4]. However, these techniques may result in under- or over-estimation of PCSA as variation of FL and PA throughout the muscle volume cannot be captured [2, 11]. In contrast, cadaveric studies have been used to model skeletal muscle at the fascicular level and to quantify architectural parameters from volumetrically digitized data [13, 14, 10]. This technique accounts for architectural variation within the muscle volume. Three-dimensional cadaveric models at the fascicular level, can be used to develop detailed ultrasound (US) protocols for investigation of *in vivo* muscle architecture. To date, it has only been possible to quantify *in vivo* PCSA using generalized 2D architectural data obtained from individual ultrasound scans. The feasibility of integrating *in vivo* imaging data with 3D cadaveric data to estimate *in vivo* PCSA has not been previously explored.

The purpose of our study is to develop a computational approach to quantify PCSA *in vivo* by integrating 3D cadaveric models with *in vivo* US data. We hypothesize that 3D *in vivo* muscle architecture can be approximated by fitting 3D cadaveric data onto 2D *in vivo* US data. This hypothesis is based on the assumption that inter-subject variability can be globally estimated

by representative geometric measurements, such as cross-sectional area and muscle length.

In this paper, 3D cadaveric data of the muscle surface and fascicle trajectory are referred to as the source data and the 2D *in vivo* US data as the target data. Corresponding features including muscle length, cross-sectional area and 2D fascicle orientation, are extracted from both data sets and compared to determine geometric differences. To integrate the two data sets, the geometric differences are minimized by fitting the source data into the target data. The fitted model is then used to estimate the *in vivo* PCSA of US imaged muscle.

2. Methods

The supraspinatus muscle was used to develop the computational approach to quantify PCSA *in vivo*. US data were acquired by scanning five live subjects (mean age: 36.4 ± 12.7) and cadaveric data were obtained from seven male formalin embalmed specimens (mean age: 61.9 ± 16) using dissection and digitization. All subjects and specimens had no supraspinatus pathology.

2.1. In vivo ultrasound data

An HDI 5000 Advanced Technology Laboratories (ATL) real-time ultrasound scanner with a linear (38 *mm*) 12 MHz transducer (resolution 0.3 *mm*) was used to scan all subjects in relaxed states, with respect to the protocol developed by Kim et al. [8]. A longitudinal image was obtained by positioning the probe at the anterior region of the muscle and aligning it to the intramuscular tendon. Three transverse images were captured by aligning the probe to the sagittal plane and positioning it at $\frac{1}{4}$, $\frac{1}{2}$ and $\frac{3}{4}$ of muscle length. The intramuscular tendon and the observed fascicles were manually determined by superimposing lines onto the longitudinal image. Anatomical cross-sections of the muscle were also manually digitized by smooth curves in the transverse images (see Figure 1).

2.2. Cadaveric data

Supraspinatus was exposed by removing the overlying skin, fascia and muscles. Shoulder joint was stabilized in neutral (anatomical position) with metal plates. Three reference points, demarcated with screws, were digitized at each level of dissection to enable 3D volumetric reconstruction of the data. The fascicles on superficial surface of muscle were delineated between

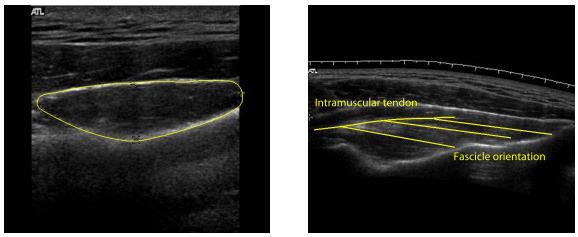

(a) (b)

Figure 1: *In-vivo* ultrasonographic assessment for the supraspinatus: (a) Segmented cross-sectional area of the transverse image. (b) Sampled fascicles and intramuscular tendon of the longitudinal image.

attachment sites using a dissecting microscope and digitized at 5–10 mm interval using a MicroScribe G2 digitizer (0.23 mm accuracy). The digitized fascicles were removed to expose underlying fascicles. This process was repeated until all fascicles (729 to 1750 per muscle) were digitized throughout the muscle volume.

Using the method developed by Lee et al. [10, 9], digitized fascicle data were geometrically reconstructed and analyzed. To be consistent with US data, one longitudinal and three transverse sections were generated from the reconstructed model by using the simulated ultrasound [9] positioned at the corresponding locations (see Figure 2).

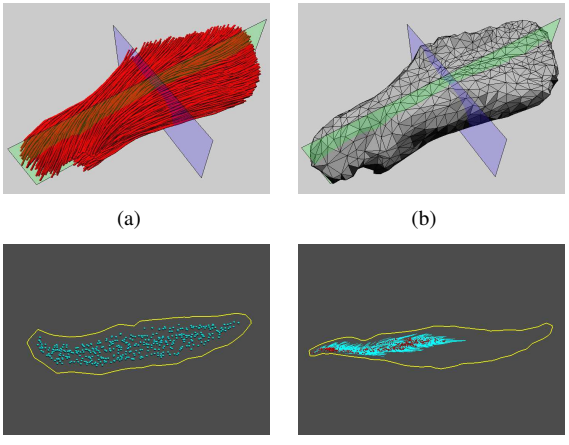

(a) (b)

(c) (d)

Figure 2: Cadaveric data of the supraspinatus: (a,b) Reconstructed architecture and surface with the transverse (mid-sagittal) and mid-longitudinal planes. (c) Cross-section image produced by the intersection of the transverse plane and the muscle geometry. (d) Longitudinal image produced by the intersection of the mid-longitudinal plane and the muscle geometry. Contour outlines (yellow), fascicles (cyan) and distribution of distal attachment (red) are shown in images (c) and (d).

2.3. Integration of cadaveric and ultrasound data

Corresponding features, such as muscle length, average cross-sectional area and fascicle orientation, are determined from 3D cadaveric data (source) and 2D US data (target) and compared to determine geometric differences. These differences are minimized by transforming cadaveric data to fit into US data. The transformed data is used to estimate PCSA of the target data.

To validate the PCSA determined by our integration method, two experiments were conducted. For experiment 1, four synthetic data were created; two cylindrical models with uniform parallel fascicle arrangement and two ellipsoidal models with uniform bipennate fascicle arrangement were created using parametric equations (See Figure 3). By cross-matching one model with the other model (i.e., $\text{parallel}_i \rightarrow \text{parallel}_j$ and $\text{bipennate}_i \rightarrow \text{bipennate}_j$ for $i \neq j$), the architectural data were transformed accordingly. For experiment 2, the seven cadaveric supraspinatus models were cross-matched in all combination ($S_i \rightarrow S_j$ and $S_j \rightarrow S_i$ for $i \neq j$). To be consistent with the method, one longitudinal and three transverse sections generated from the target model were used to transform the source model. The relative error (%) between PCSA of the transformed model (i.e., $\text{PCSA}_{s\rightarrow t}$) and that of the target model was calculated to assess the fidelity of our method (i.e., $(\text{PCSA}_{s\rightarrow t} - \text{PCSA})/\text{PCSA}$).

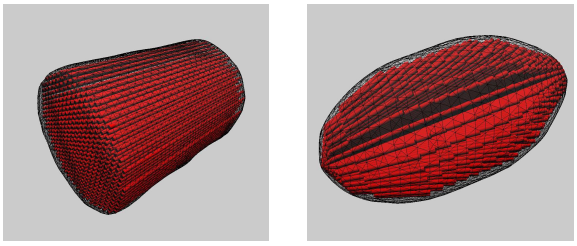

(a) (b)

Figure 3: Synthetic muscles. (a) Parallel muscles are created within a cylinder; parallel_1 (length of 20 mm and radius of 12 mm) and parallel_2 (length of 20 mm and radius of 10 mm). (b) Bipennate muscles are created within an ellipsoid; bipennate_1 (length of 25 mm, width of 13 mm, height of 13 mm and pennation angle of 20°) and bipennate_2 (length of 20 mm, width of 10 mm, height of 10 mm and pennation angle of 25°).

2.4. Transformation between muscle models

We relate two ways (cf. (1) and (2)) to represent muscle volume, which allows us to explicitly associate the architecture with the external measurement (e.g., cross-sectional area and muscle length) per muscle. The difference in this measurement is then used to approximate architectural variation between muscles. By minimizing this difference, architecture of one muscle (referred to as source muscle) is fitted to that of the other muscle (referred to as target muscle).

In a cadaveric muscle, the volume of each fascicle is approximately modeled by a cylinder along its trajectory. As the entire muscle architecture is represented by a collection of those cylinders, the muscle volume (MV) can be estimated by

$$\text{MV} = \sum_{i=1}^{n} a_i l_i \tag{1}$$

where a_i is the cross-sectional area of fascicle i, l_i is the length of fascicle i and n is the number of fascicles. Since the reconstructed surface encloses all fascicles, the overall muscle volume is thus approximated by summing the product of cross-sectional slices by their thickness:

$$\text{MV} = \sum_{k=1}^{m} c_k \Delta h = \sum_{k=1}^{m} c_k \frac{h}{m} = \bar{c} h \tag{2}$$

Here, c_k is a cross-sectional area of k-th slice of the muscle, m is the number of cross-sections, h is the length of the muscle, $\Delta h = \frac{h}{m}$ is the average thickness of each cross-section and $\bar{c} = \frac{1}{m}\sum_{k=1}^{m} c_k$ is the average cross-sectional area. Using (2), the inter-subject variability of muscle volume can be approximated. For a target muscle having volume MV^t and source muscle having volume MV^s, let $\alpha = \frac{\text{MV}^t}{\text{MV}^s}$ be the scaling factor between the target and source muscles. Then α can be estimated as the product of relative cross-sectional area (α_c) and length (α_h) between muscles:

$$\alpha = \alpha_c \alpha_h,\ \alpha_c = \frac{\bar{c}^t}{\bar{c}^s},\ \alpha_h = \frac{h^t}{h^s} \tag{3}$$

where $\bar{c}^s$ and $\bar{c}^t$ are the average c_k of the source and target muscles, respectively, and h^s and h^t are the length of the source and target muscles, respectively. Using the results above, the volume of the target muscle can be rewritten in terms of the architecture of source muscle as

$$\text{MV}^t = \sum^{n^t} a_i^t\, l_i^t = \alpha_c \alpha_h \sum^{n^s} a_i^s\, l_i^s \tag{4}$$

where superscripts s and t indicate the source and target muscles, respectively. Since the $\bar{c}$ and h values can be measured from both cadaveric and ultrasonographic

assessments, it is straightforward to determine α_c and α_h. The values of α_c and α_h are used to explicitly transform the source muscle so that its volume approximates the volume of the target muscle. For simplicity, the transformation is decomposed into transverse and longitudinal transformations. The transverse transformation minimizes the difference in the cross-sectional areas between the source and the target muscles, whereas the longitudinal transformation is used to match the lengths of the muscles.

2.4.1. Transverse transformation

A 3D geometry of the target muscle is approximated by either shrinking or expanding that of the source muscle. For simplicity, the transformation is restricted to the transverse plane. The amount of shrinkage or expansion is determined by the scaling factor, α_c in (3), which we use to minimize the difference in the cross-sectional areas between the source and the target muscles. In transverse ultrasound images, the cross-sectional area of a muscle is approximated by a polygon, the area of which is calculated by manual digitization. The value of $\overline{c}^t$ is obtained by averaging cross-sectional areas, c_k^t, estimated from three transverse images.

For each cross-section C_k^s ($k = 1, 2, 3$), its nearby vertices on the surface are identified as G_k to constitute $G = \bigcup_k G_k$. Since the transformation is restricted to the transverse plane and it is uniform around the surface, new position for vertices in G can be simply defined by symmetrically displacing them inward or outward from the surface. The amount of displacement is determined so that the associated cross-sectional area can be transformed to achieve the target value; $c_k^{s'} = \alpha_c c_k^s$. Since the cross-section is represented by a closed polygon having a number of boundary points, its area is calculated as

$$c_k^s = \frac{1}{2} \sum_{i=1}^{n^e} \mathbf{n}_t \cdot (\mathbf{p}_i - \mathbf{x}_o) \times (\mathbf{p}_{i+1} - \mathbf{x}_o) \tag{5}$$

where $\mathbf{n}_t$ is a normal of the transverse plane, $\mathbf{x}_o$ is an arbitrary point on that plane, n^e is the number of edges representing the boundary of the cross-section, and $\mathbf{p}_i$ and $\mathbf{p}_{i+1}$ are the end points on the edge i. These boundary points $\mathbf{p}$ are determined by the intersection of the transverse plane and the muscle surface. Likewise, new cross-sectional area is calculated in terms of the displacement from the original points:

$$c_k^{s'} = \frac{1}{2} \sum_{i}^{n^e} \mathbf{n}_t \cdot (\mathbf{p}'_i - \mathbf{x}_o) \times (\mathbf{p}'_{i+1} - \mathbf{x}_o) \tag{6}$$

$$\mathbf{p}'_i = \mathbf{p}_i + \Delta r_k \mathbf{t}(\mathbf{p}_i) \tag{7}$$

where $\mathbf{t}(\mathbf{p}_i)$ is the unit vector representing the normal traction at $\mathbf{p}_i$ and Δr_k is the displacement along the traction. Substituting (7) into (6), we solve for Δr_k to make (6) equal to the target value $c_k^{s'} = \alpha_c c_k^s$ ($k = 1, 2, 3$). Similar to (7), new positions for vertices in G_k are determined by using Δr_k:

$$\mathbf{u}_i = \mathbf{v}_i + \Delta r_k \mathbf{t}(\mathbf{v}_i) \tag{8}$$

where $\mathbf{t}(\mathbf{v}_i)$ is the unit vector representing the normal traction at $\mathbf{v}_i$ (see Figure 4).

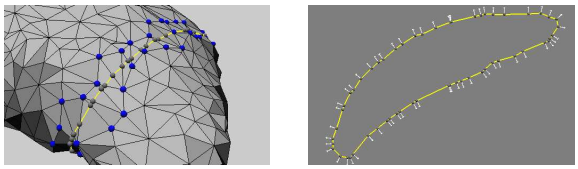

(a) (b)

Figure 4: Displacement for transverse transformation: (a) Cross-section C_k^s (yellow) with boundary points, $\mathbf{p}$ (gray), and adjacent vertices, G_k (blue), subject to the constraint in the transformation. (b) 2D view of cross-section with the displacement (white).

The muscle surface is reconstructed based on the enclosed fascicles, the trajectories of which directly represent geometric details of the surface. This geometric correspondence between the surface and fascicle arrangement is used to approximate the new architecture associated with the transformed surface. Thus, geometric surface details must be preserved as much as possible during the transformation. To this end, we use the Laplacian surface deformation technique [17] because it allows us to effectively transform global shape while preserving local details. These details are represented by the Laplacian coordinates that capture the difference between the vertex and the average of its neighboring vertices:

$$\delta_i = \mathcal{L}(\mathbf{v}_i) = \mathbf{v}_i - \frac{1}{d_i} \sum_{j \in N_i} \mathbf{v}_j \tag{9}$$

where N_i is the set of vertices adjacent to $\mathbf{v}_i$ and d_i is the number of elements in N_i. The surface is transformed

by constraining a set of vertices to the desired positions and fitting the Laplacian coordinates of new surface $\mathbf{v}'$ to the initial Laplacian δ of the original surface $\mathbf{v}^o$:

$$\mathbf{v}' = \arg\min_{\mathbf{v}}(\|\mathcal{L}(\mathbf{v}) - \delta\|^2 + \sum_{i\in G} \omega_i \|\mathbf{v}_i - \mathbf{u}_i\|^2) \quad (10)$$

where

$$\begin{aligned} \mathcal{L}(\mathbf{v}) &= (\mathcal{L}(\mathbf{v}_1), \mathcal{L}(\mathbf{v}_2), ..., \mathcal{L}(\mathbf{v}_n))^T, \\ \delta &= \mathcal{L}(\mathbf{v}^o) = (\delta_1, \delta_2, ..., \delta_n)^T, \\ n &: \text{the number of vertices on the surface} \end{aligned}$$

G is a set of vertices subject to the constraint during the transformation, $\mathbf{u}_i$ is the positional constraint (i.e., desired position) for $\mathbf{v}_i$ by (8) and ω_i is its weight.

The supraspinatus is a pennate muscle for which fascicles originate from the broad proximal region and insert into the narrow distal region. With this convergent fascicle orientation, their distal attachment exhibits strong linearity along the intramuscular tendon. Since the surface transformation determines the internal fascicle arrangement, a large transformation (e.g., $\alpha_c \ll 1$ or $\alpha_c \gg 1$) may perturb the architectural pattern that needs to be preserved. To this end, we use an additional static constraint ($\mathbf{u}_i = \mathbf{v}_i$) that restricts the movement of the vertices wrapping around the distal tendon. By incorporating this static constraint, (10) is expanded as

$$\mathbf{v}' = \arg\min_{\mathbf{v}}(\|\mathcal{L}(\mathbf{v})-\delta\|^2+\sum_{i\in G} \omega_i \|\mathbf{v}_i-\mathbf{u}_i\|^2)+\sum_{j\in S} \omega_j \|\mathbf{v}_j-\mathbf{u}_j\|^2) \quad (11)$$

where S is a set of vertices constituting the distal tendon area on the muscle surface.

While the surface is transformed by (11), the enclosed fascicles need to be transformed similarly, ensuring that the appropriate geometry is maintained (see Figure 5). To this end, we use the generalized mean value coordinates technique [7], the common application of which is to manipulate object deformation by means of a surrounding control mesh. This technique geometrically associates the vertices of an arbitrary object with those of a control mesh, which embraces the construction of a weight function, w (namely, mean value coordinates) having the following properties: continuity, smoothness and linear precision. For a detailed description of this technique, the reader is referred to Ju et al. [7]. For our purpose, the enclosed fascicles and their surrounding surface are considered to be the deformable object and the control mesh, respectively. For every fascicle point $\mathbf{x}_j$, its mean value coordinates w_i are computed with respect to each vertex $\mathbf{v}_i$ in the original surface (i.e., prior to the transformation) and set as constant during the transformation. By letting $\mathbf{v}'_i$ be the positions of the vertices from the transformed surface, the new interior fascicle point, $\mathbf{x}'_j$ in the enclosing surface is computed as

$$\mathbf{x}'_j = \frac{\sum_i^n w_{ij}\mathbf{v}'_i}{\sum_i^n w_{ij}} \quad (12)$$

where n is the number of vertices on the surface, w_{ij} is the mean value coordinate described in [7], for $\mathbf{x}_j$ and $\mathbf{v}_i$.

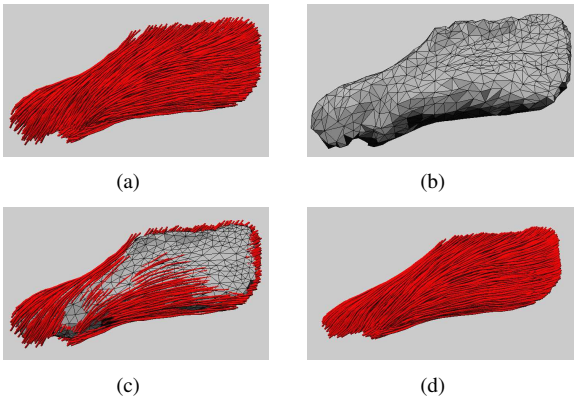

Figure 5: Transverse transformation for the supraspinatus: (a,b) Architecture (red) and its enclosing surface (gray). (c) Transformed surface (gray) with respect to specified constraints. (d) Transformed architecture (red) corresponding to the transformed surface.

2.4.2. *Longitudinal transformation*

The longitudinal transformation not only matches the length of the muscles, but also minimizes the PA difference between the muscles. In contrast to the transverse transformation, it is directly applied to the fascicle arrangement because it is straightforward to adjust the length and the angle based on the fascicle trajectory. To minimize the perturbation of the tendinous attachment, the transformation is restricted to the direction of the intramuscular tendon. While fascicles are fixed at the proximal attachment, they are elongated or shortened by translating their distal attachment along the tendon direction (see Figure 6). Similar to (10), a least-squares-based optimization is used to transform the fascicle trajectory while preserving local curvatures. Associated translational displacements (Δh_1 and Δh_2) are specified with respect to the scaling factor in (3), and PA measurement, respectively.

$$\Delta h_1 = \alpha_h h^s - h^s \tag{13}$$

$$\Delta h_2 = \arg\min_{\Delta h} \left(\sum_i^{n^f} \cos^{-1} \left(\mathbf{a}^s \cdot \frac{(\mathbf{t}_i^s + \Delta h\, \mathbf{a}^s)}{\|(\mathbf{t}_i^s + \Delta h\, \mathbf{a}^s)\|} \right) - \overline{\mathrm{PA}}_{2D}^{t} \right)^2 \tag{14}$$

where n^f is the number of fascicles in the source muscle visible by the simulated ultrasound, $\mathbf{a}^s$ is the direction of the intramuscular tendon, $\mathbf{t}_i^s$ is the tangent of fascicle i at the distal attachment in the source muscle and $\overline{\mathrm{PA}}_{2D}^{t}$ is the average PA of fascicles sampled on the imaging plane in the target muscle. Their proximity to that plane is evaluated to identify visible portions of fascicles. All parameters given in (14) are based on 2D measurement. The US approach accounts for three fascicles sampled at the most proximal, middle and most distal locations of the intramuscular tendon, which approximate the PA distribution of the target muscle in 2D. In contrast, the cadaveric approach takes into account all visible fascicles for angular measurement in (14). The transformation is carried out in two steps: translation of distal attachments by (13) and then by (14). The transformation by Δh_2 may alter the muscle length, but it is not critical in our problem, because PCSA estimation is not dependent on the length.

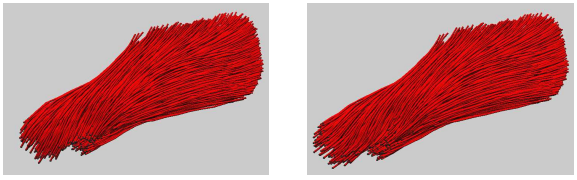

(a) (b)

Figure 6: Longitudinal transformation for the supraspinatus: (a) Original architecture. (b) Transformed architecture with respect to translation of distal attachments.

3. Results

As described in Section 2.3, three experiments were performed. Experiment 1 and 2 (synthetic and cadaveric data, respectively) are based solely on the three-dimensional data, whereas experiment 3 uses 3D cadaveric data and 2D US data. When both the target model and the transformed model have 3D fascicle data (experiment 1 and 2), their PCSA can be determined using the method described in [10]. Measurements for those data are given in Table 1. The PCSA calculated solely from the 3D data is regarded as the true value and compared against the PCSA computed by our fitting method from the 3D to 2D data ($\mathrm{PCSA}_{s\to t}$). Our results for the PCSA estimation are presented in Tables 2, 3 and 4, respectively.

3.1. Experiment 1: Synthetic data

For parallel muscles, the relative differences in PCSA between $\mathrm{parallel}_1$ and $\mathrm{parallel}_2$ before the transformation, are 41.8% and −29.5%, respectively. After the transformation, those differences are significantly reduced to −1.5% and −2.5%, respectively. Similarly, for bipennate muscles, the relative differences in PCSA between $\mathrm{bipennate}_1$ and $\mathrm{bipennate}_2$ are significantly lowered from 55.6% to −0.6% and −35.7% to −7.5%, respectively. Results show that our method performs slightly better when the muscle surface shrinks than when it expands, where by shrink we mean that the source muscle has a bigger PCSA than the target muscle. Recall that fascicles located in the outermost layers have some degree of deficiency in that they are surrounded by a few neighboring fascicles only, not completely enclosed by them. That may result in an unbounded Voronoi region, the area of which must be extrapolated or discarded, depending on the deficiency. Generally, shrinking the muscle improves this deficiency problem by increasing the density of fascicle points inside the muscle. On the other hand, expanding the muscle disperses these points, making the problem described above for the outermost regions worse. Consequently this may yield a less accurate estimation.

Muscle	N	h	$\overline{c}$	PA_{2D}	PCSA
$\mathrm{parallel}_1$	390	20.0	453.9	0.0	448.7
$\mathrm{parallel}_2$	154	20.0	334.5	0.0	316.5
$\mathrm{bipennate}_1$	891	25.0	173.2	16.6	162.8
$\mathrm{bipennate}_2$	750	20.0	115.3	13.4	104.6
S_1	1750	134.2	622.2	6.7	647.0
S_2	729	115.6	424.5	4.4	421.3
S_3	1081	125.9	506.6	8.3	543.8
S_4	1681	135.1	571.5	7.6	613.0
S_5	1294	131.7	698.3	7.5	694.8
S_6	1556	138.6	798.5	6.9	847.0
S_7	829	125.8	416.1	6.3	417.2
US_1	–	111.4	625.8	11.7	–
US_2	–	88.5	549.4	8.4	–
US_3	–	81.2	503.2	11.8	–
US_4	–	99.1	433.9	14.3	–
US_5	–	97.1	515.1	8.9	–

Table 1: Measurements for synthetic, cadaveric and US data. N is the total number of digitized fascicles. h is the longitudinal length of muscle (mm). $\overline{c}$ is the mean cross-sectional area (mm^2). PA_{2D} is the mean pennation angle of fascicles projected onto the mid-longitudinal plane. PCSA is estimated based on the original fascicle data (mm^2). Note that N and PCSA are unknown in US data.

Muscle$_s$ \ Muscle$_t$	parallel$_1$	parallel$_2$	bipennate$_1$	bipennate$_2$
parallel$_1$		311.6 (−1.5)		
parallel$_2$	437.6 (−2.5)			
bipennate$_1$				103.9 (−0.6)
bipennate$_2$			150.5 (−7.5)	

Table 2: PCSA estimation (PCSA$_{s\to t}$) for synthetic muscles. PCSA$_{s\to t}$ is estimated by mapping the architecture from Muscle$_s$ (source muscle) to Muscle$_t$ (target muscle). The relative errors, expressed as percentages, are given in parenthesis.

3.2. Experiment 2: Cadaveric data

From the seven specimens, 42 ordered-pairs are selected to perform the experiment ($\mathcal{T}_{i,j} : S_i \to S_j, i \neq j$). The PCSA of the transformed source muscle is estimated by our method and compared with that of the target muscle. Specimens yield a wide range of absolute relative errors (for instance, 0.7 % for $\mathcal{T}_{1,3}$ to 15.2 % for $\mathcal{T}_{1,2}$). This is mainly due to the architectural complexity and the variation between specimens. It is observed that the supraspinatus has non-uniform architecture: bipennate in the anterior region and parallel in the posterior region. Depending on the distribution of the fascicle orientation (i.e., the pennation angle) and the relative thickness of these regions, PCSA may be larger than $\overline{c}$ (e.g., S_1, S_3, S_4 and S_6) or comparable to $\overline{c}$ (e.g., S_2, S_5 and S_7). Since the muscle architecture is not significantly altered in our method, this discrepancy between PCSA and $\overline{c}$ may persist during the mapping. It is also found that some mappings that induce a large shrinkage, such as $\mathcal{T}_{1,2}$, $\mathcal{T}_{1,7}$, $\mathcal{T}_{6,2}$ and $\mathcal{T}_{4,7}$, yield more inaccurate results (above 12.0 %) than others do (below 8.0 %). This is caused by our static constraints specified to prevent undesired geometric changes and perturbations of the intramuscular tendon. Recall that the displacement for the mapping is determined by the difference between mean cross-sectional areas of muscles. The bigger the difference, the larger the displacement needed to transform the entire surface. However, too large a displacement may collapse the narrow distal region of the muscle volume or affect the linearity of an intramuscular tendon. In such cases, the associated static constraints adversely affect the transformation. As a result, the PCSA may not reach the targeted value. As PA_{2D} variation is relatively small in this experiment, it is observed that, compared to the transverse transformation, the longitudinal transformation has little effect on estimating the PCSA.

Statistical analysis of the estimated PCSA is also presented in Table 3. Depending on architectural variation and volumetric differences between source and target muscles, the transformation can under- or over-estimate PCSA. However, compared to the distribution of original PCSA for all specimens (standard deviation: ±153.2), that of the estimated PCSA for each target muscle is much narrower (standard deviation: ±24.6 ∼ ±35.7). Furthermore, it is shown that the mean of each distribution ($\overline{\text{PCSA}}_{s\to t}$) is much closer to the true PCSA of the corresponding target muscle (−5.1 % ∼ 8.4 %) than that of the original PCSA distribution (−29.4 % ∼ 43.3 %).

3.3. Experiment 3: Cadaveric data to US data

In contrast to the previous two experiments, it is impossible to validate our estimation in this experiment, because the PCSA of the target muscles are unknown. Thus, only statistical results from experiments on all pairs of muscles are presented in Table 4. Similar to experiment 2, lower and upper bounds on the PCSA estimation are determined by the smallest and the largest source muscles, respectively. Also, the distribution of the estimated PCSA per target muscle is narrow (standard deviation: ±23.7 ∼ ±29.0), which indicates that the mean estimates based on cadaveric data can be a practical approximation of *in vivo* PCSA for US imaged muscles.

4. Discussion

An accurate determination of PCSA is needed for both biomechanical and clinical studies because reliable functional analysis and associated clinical assessment are highly dependent on the quality of this measure. *In-vivo* studies based on MRI and ultrasonography may under- or over-estimate PCSA because architectural complexity and variation are rarely accounted for. On the other hand, cadaveric modeling cannot be directly applied to *in vivo* studies. Therefore, the purpose of our study is to overcome the limitations inherent in each approach by combining them to produce accurate quantification method for PCSA calculation for *in-vivo* muscle. To this end, subject-specific architecture is approximated by fitting a 3D detailed reference architecture model (cadaveric data) to the target muscle

Muscle$_s$ \ Muscle$_t$	S_1	S_2	S_3	S_4	S_5	S_6	S_7
S_1		485.6 (15.2)	539.9 (0.7)	618.9 (0.9)	716.3 (3.1)	855.5 (1.0)	470.5 (12.7)
S_2	603.4 (−6.7)		484.9 (−10.8)	547.8 (−10.6)	664.7 (−4.3)	758.8 (−10.4)	403.1 (−3.4)
S_3	618.6 (−4.4)	426.5 (1.2)		580.7 (−5.2)	652.7 (−6.0)	790.1 (−6.7)	412.4 (−1.1)
S_4	658.4 (1.7)	471.4 (11.9)	548.1 (0.8)		721.3 (3.8)	822.6 (−2.8)	476.6 (14.2)
S_5	635.9 (−1.7)	441.2 (4.7)	527.2 (−3.0)	586.0 (−4.4)		803.7 (−5.1)	434.7 (4.2)
S_6	670.2 (3.6)	478.3 (13.5)	558.6 (2.7)	622.6 (1.6)	744.8 (7.2)		464.0 (11.2)
S_7	615.4 (−4.8)	437.6 (3.9)	500.9 (−7.8)	564.6 (−7.8)	685.0 (−1.4)	791.6 (−6.5)	
$\overline{\text{PCSA}}_{s\to t}$	633.6 ± 26.2	456.8 ± 24.6	526.6 ± 28.5	586.8 ± 29.5	697.6 ± 35.7	803.7 ± 32.8	443.6 ± 31.4
PCSA	647.0	421.3	543.8	613.0	694.8	847.0	417.2
Error (%)	−2.1	8.4	−3.2	−4.3	0.4	−5.1	6.3

Table 3: PCSA estimation ($\text{PCSA}_{s\to t}$) for cadaveric specimens. $\text{PCSA}_{s\to t}$ is the estimated PCSA for Muscle_t (target muscle) computed by mapping the architecture of Muscle_s (source muscle) to the 2D ultrasound version of Muscle_t. The percentage of the relative errors of $\mathcal{T}_{i,j}$ are given in parenthesis. Statistical analysis of $\text{PCSA}_{s\to t}$ for each Muscle_t is given as 'the mean ± the standard deviation'.

Muscle$_s$ \ Muscle$_t$	US_1	US_2	US_3	US_4	US_5
S_1	651.2	583.1	528.4	468.8	555.5
S_2	603.0	551.0	498.1	432.7	517.8
S_3	640.5	560.4	527.8	459.7	542.8
S_4	662.7	587.6	540.6	470.3	555.0
S_5	624.1	545.8	505.6	444.4	516.9
S_6	677.9	603.3	553.8	483.7	569.2
S_7	602.7	541.8	482.3	403.9	490.2
$\overline{\text{PCSA}}_{s\to t}$	637.4 ± 29.0	567.6 ± 23.7	519.5 ± 25.2	451.9 ± 27.2	535.4 ± 27.9

Table 4: PCSA estimation ($\text{PCSA}_{s\to t}$) for *in-vivo* supraspinatus of living subjects.

that is represented by 2D geometric measures (US data). This approximate architecture model is used for PCSA quantification. Two validation experiments based on synthetic muscle and cadaveric specimens, respectively, demonstrate 0.4 − 8.4 % errors between original architecture and its approximation, depending on the anatomical complexity. No error analysis is conducted in the third experiment based on cadaveric and US data because their exact PCSA is unknown. Nevertheless, the distribution of estimation results provides a practical insight into *in-vivo* quantification of PCSA.

Our approach can not only be used for static analysis, but it can also be applied to an investigation of dynamic problems associated with muscle contraction or skeletal movement. A variable range of muscle activity can be assessed similarly in terms of 2D geometric measures in the ultrasound images. Thus, one possible extension of our method is to quantify changes of architectural parameters during muscle contraction. Another possible application is to provide region-specific architectural analysis for *in-vivo* muscle, such as the anterior/posterior or the superficial/deep region. This may need only an additional localization in the ultrasonographic assessment because our architectural model can be easily re-organized into multiple layers or regions.

Although our study provides improved capability for *in-vivo* PCSA estimation, there are some limitations that may be addressed in future work. First, in the present study, we considered only a small sample of data. A more thorough validation needs more specimens and a variety of types of muscle. Second, the gap between superficial fascicles and the muscle surface may lead to a significant error, particularly when the muscle expands, because this gap is proportionally scaled with the amount of transformation. Thus, minimizing this gap, by possibly using a tighter surface, could further reduce the estimation error. Lastly, performance of our method is highly sensitive to the consistency between cadaveric and US data, such as the orientation and location of their imaging planes. The present study uses only the proximal to distal length of the muscle to compare images. Additional image features, such as shape of cross-sections and bony landmarks, may enhance the reliability to our method.

Acknowledgement

This research was supported in part by the Natural Sciences and Engineering Research Council (NSERC) of Canada and the GRAND NCE of Canada.

Conflict of interest statement

We hereby declare that no conflict of interest exists in our study.

Reference

[1] Alexander, R., Vernon, A., 1975. The dimensions of knee and ankle muscles and the forces they exert. Journal of Human Movement Studies 1, 115–123.

[2] Bénard, M., Becher, J., Harlaar, J., Huijing, P., Jaspers, R., 2009. Anatomical information is needed in ultrasound imaging of muscle to avoid potentially substantial errors in measurement of muscle geometry. Muscle Nerve 39, 652–665.

[3] Branda, R., Pedersen, D.R., Friederich, J.A., 1986. The sensitivity of muscle force predictions to changes in physiologic cross-sectional area. Journal of Biomechenics 19, 589–596.

[4] Dupont, A., Sauerbrei, E., Fenton, P., Shragge, P., Loeb, G., Richmond, F., 2001. Real-time sonography to estimate muscle thickness: comparison with MRI and CT. Journal of Clinical Ultrasound 29, 230–236.

[5] Fukunaga, T., Ichinose, Y., Ito, M., Kawakami, Y., Fukashiro, S., 1997a. Determination of fascicle length and pennation in a contracting human muscle in vivo. Journal of Applied Physiology 82, 354–358.

[6] Fukunaga, T., Kawakami, Y., Kuno, S., Funato, K., Fukashiro, S., 1997b. Muscle architecture and function in humans. Journal of Biomechanics 30, 457–463.

[7] Ju, T., Schaefer, S., Warren, J., 2005. Mean value coordinates for closed triangular meshes. ACM Trans. Graph. 24, 561–566.

[8] Kim, S., Bleakney, R., Boynton, E., Ravichandiran, K., Rindlisbacher, T., McKee, N., Agur, A., 2010. Investigation of the static and dynamic musculotendinous architecture of supraspinatus. Clinical Anatomy 23, 48–55.

[9] Lee, D., Li, Z., Sohail, Q.Z., Jackson, K., Fiume, E., Agur, A., 2014. A three-dimensional approach to pennation angle estimation for human skeletal muscle. Computer Methods in Biomechanics and Biomedical Engineering 18, 1474–1484.

[10] Lee, D., Ravichandiran, K., Jackson, K., Fiume, E., Agur, A., 2012. Robust estimation of physiological cross-sectional area and geometric reconstruction for human skeletal muscle. Journal of Biomechanics 45, 1507–13.

[11] Namburete, A.I., Rana, M., Wakeling, J.M., 2011. Computational methods for quantifying in vivo muscle fascicle curvature from ultrasound images. Journal of Biomechanics 44, 2538–2543.

[12] Narici, M., 1999. Human skeletal muscle architecture studied in vivo by non-invasive imaging techniques: functional significance and applications. Journal of Electromyography and Kinesiology 9, 97–103.

[13] Ravichandiran, K., Ravichandiran, M., Oliver, M., Singh, K., McKee, N., Agur, A., 2009. Determining physiological cross-sectional area of extensor carpi radialis longus and brevis as a whole and by regions using 3d computer muscle models created from digitized fiber bundle data. Comput. Methods Prog. Biomed. 95, 203–212.

[14] Ravichandiran, K., Ravichandiran, M., Oliver, M., Singh, K., McKee, N., Agur, A., 2010. Fibre bundle element method of determining physiological cross-sectional area from three-dimensional computer muscle models created from digitised fibre bundle data. Comput. Methods Prog. Biomed. 13, 741–748.

[15] Sacks, R., Roy, R., 1982. Architecture of the hindlimb muscles of cats: functional significance. Journal of Morphology 173, 185–195.

[16] Scott, S., Engstrom, C., Loeb, G., 1993. Morphometry of human thigh muscles. Determination of fascicle architecture by magnetic resonance imaging. Journal of anatomy 182, 249–257.

[17] Sorkine, O., Cohen-Or, D., Lipman, Y., Alexa, M., Rössl, C., Seidel, H.P., 2004. Laplacian surface editing, in: Proceedings of the 2004 Eurographics/ACM SIGGRAPH symposium on Geometry processing, ACM, New York, NY, USA. pp. 175–184.